Experimental and Numerical Investigation of Strength of Inertial Entrainment

A Thesis submitted in partial fulfilment of the requirements for the Degree of

Bachelor of Technology

in

Mechanical Engineering

by

Priyanka Agrawal (Roll No. 110ME0439)

Nitish Varma (Roll No. 110ME0343)

Under the guidance of

Dr. Suman Ghosh

Department of Mechanical Engineering
National Institute Of Technology
Rourkela – 769008

National Institute of Technology Rourkela

CERTIFICATE

This is to certify that the research work that has been presented in this thesis entitled "**Experimental and Numerical Investigation of Strength of Inertial Entrainment**" by Priyanka Agrawal (Roll No.110ME0439) and Nitish Varma (Roll. No.110ME0343), has been carried out under my supervision in partial fulfilment of the requirements for the degree of Bachelor of Technology in Mechanical Engineering during session 2013-2014 in the Department of Mechanical Engineering, National Institute of Technology, Rourkela.

To the best of my knowledge, this dissertation work has not been submitted in any other college or university at any time prior to this, for the award of any degree or diploma.

Place: Rourkela
Date:

Dr. Suman Ghosh
Assistant Professor
Department of Mechanical Engineering
National Institute of Technology, Rourkela

ACKNOWLEDGEMENT

We would like to extent our heartfelt indebtedness to Dr. Suman Ghosh, Department of Mechanical Engineering, N.I.T Rourkela, for giving us this opportunity to work under him. Like a true mentor, he has supported and guided us in every step and also helped us to tackle every problem faced during the project. We find ourselves grateful to have him as our mentor.

We would also like to thank Dr. K. P. Maity, H.O.D, Department of Mechanical Engineering, N.I.T Rourkela, for allowing us to work in lab for extended duration and granting access to departmental facilities.

Priyanka Agrawal

110ME0439

Nitish Varma

110ME0343

Contents

List of Figures

List of Tables

List of Graphs

List of Equations

List of Symbols

ρ	Density
v	Velocity vector
p	Pressure
g	Gravity vector
α	Volume fraction
m_{pq}	Mass transferred from phase p to phase q
m_{qp}	Mass transferred from phase q to phase p

1 INTRODUCTION AND LITERATURE REVIEW

In this section, the problem has been introduced by the detailed explanation of the phenomena and its occurrence. The practical applications of the phenomena have been discussed with the literature review covering the work that has already been done. The gaps in the literature have been pointed out and the aims and objectives of the present work, in accordance with the gaps found, have been listed.

1.1 Introduction

Entrainment is a multiphase phenomenon. It is the process of drawing away of one fluid because of the motion of another fluid or body. When one fluid moves through another fluid, it tends to drag the other fluid with it. This dragging can be observed when an air bubble moving upwards in a fluid tries to break through the surface and it splashes the liquid. This happens so because the momentum of the air bubble caused the liquid to move upwards with it. The surface tension of the liquid prevents it from breaking off the surface. Entrainment of air into liquid is observed when filling a bucket with water from a tap. The air around the surface of the water where the stream of the tap is present gets sucked into the water with the flow of stream from the tap.

In this work the stress is laid upon inertial entrainment- entrainment caused by inertia forces. When a gas bubble is injected into a liquid, the bubble experiences an upward force due to buoyancy. If the bubble is injected into the denser liquid of a two layer stratified liquid-liquid system, the bubble tries to move upwards since density of gas is lesser than that of both liquids. As the bubble crosses the interface of the two liquids, it tries to take some of the denser liquid into the rarer liquid region. Due to momentum, a part of the denser liquid which is attached to the bubble separates from the main and

travels into the rarer liquid. Soon afterwards, due to weight the detached denser liquid separates from the bubble and travels downwards whereas the gas bubble continues to move upwards. This dragging of denser liquid into rarer liquid by the gas bubble is called inertial entrainment.

Entrainment process can be seen both in natural and artificial events. Cyclonic winds and weather storms include stratified layer of air and water phases. Many turbulent weather conditions can be explained on the basis of entrainment. Different artificial purposes also utilize the phenomenon of entrainment. One of the examples is an educator pump. These pumps are used in ships to extract water in case of water leakage into the ship. The pump is used to remove the air and the water inside the ship is entrained out by the suction of the pump. Entrainment is used for air bubble entrapment in concrete. This helps to strengthen the concrete. Entrainment is also observed in the making of emulsion of one fluid in another, such as margarine. As for artificial processes with stratified liquid layers, the best examples metal extraction industries and nuclear reactors. In both cases gases are formed within liquid layers and cause entrainment. This is unwanted as entrainment causes mixing between two liquids. However in case of desalination plants and other places where mixing is desired, entrainment is enhanced purposely. The mixing of two fluids is generally done by bubbling gas through a tank containing the two fluids. These type of systems are called gas bubble stirred tanks.

1.2 Literature Review

There is a wealth of literature present for the study of entrainment phenomenon. Much work has been done to study the various parameters, effects, and other details of the phenomenon. Investigations have been done earlier in all forms- experimental, analytical and numerical.

Liu and Peng (2014) have studied the entrainment of clay minerals in flotation. The study is done for both tap water and saline water. The entrainment of clay minerals in flotation is undesired and so the study is done to reduce the entrainment. The result is that saline water led to higher entrainment rate than tap water. Of the different types of clay minerals, Kalonite Q38 showed higher entrainment. Li et al. (2014) have studied the entrainment behavior of sericite in microcrystalline graphite flotation. Here too, the aim was to reduce the rate of entrainment. The investigation was carried out during both presence and absence of microcrystalline graphite to note its effect. The graphite was found to have high impact on the phenomenon. Oka et al. (2014) have worked to find the information on the entrainment properties of horizontally spreading ceiling jet. This is required as it helps in fire safety and rescue missions. Cristofano et al. (2014) have worked on gas entrainment onset conditions in unstable free surface vortices. They have use a specifically built gas entrainment test section for the same. Tian et al. (2014) have studied the liquid entrainment behavior at the nozzle exit in coaxial gas-liquid jets. The examination of transitional behavior observed is done. Roy et al. (2013) have investigated the visualization of air entrainment by plunging jet. The cause of entrainment is found as formation of air sheath. In churn flow, Wang et al. (2013) have proposed a mathematical-model for the drop-entrainment. The effect of parameters have been investigated and discussed. Wang et al. (2013) have again investigated the wave and drop entrainment experimentally. Kulkarni and Patwardhan (2013) have studied the phenomenon of gas entrainment in stirred tanks by CFD modelling. The onset conditions have been investigated. In a diesel engine, crevice soot entrainment have been computationally studied by Tan et al. (2013). The findings have been used to elongate the life of engines. Brouilliot and Lubin (2013) have numerically simulated entrainment of air in a plunging liquid-jet. They have developed the numerical model for classical

VOF- PLIC model. They have also used LES turbulence model. In liquid-liquid systems, Shahrokhi and Shaw (1994) have investigated the origination of drops by batch gas agitation. Their criteria was to minimize the fine drop formation. The work is experimental in nature. Greene et al. (1991) have developed analytical model for induction of bubble entrainment between stratified liquid layers. The entrainment efficiencies have been calculated. Greene et al. (1988) have also studied the strength of the entrainment by measuring the volume of entrained liquid. Different liquid pairs were used in experimental runs.

The summary of the literature review has been presented in a tabular format in **Table *1.1***.

Table 1.1: Summary of Literature Review

Title of paper	**Author**	**Publication**	**Results**
Reducing the entrainment of clay minerals in flotation using tap and saline water	Di Liu and Yongjun Peng	Powder Technology, Volume 253, February 2014, pp. 216-222	• Saline water has higher entrainment than tap water. • Kaolinite Q38 has higher entrainment in flotation. • Addition of PEO reduces the entrainment of kaolinite Q38 due to the formation of less compact flocs and higher froth stability.
The entrainment behaviour of sericite in microcrystalline graphite flotation	Hongqiang Li, Qiming Feng, Siyuan Yang, Leming Ou	Int. J. of Mineral Processing, Volume 127, March 2014, pp. 1-9.	• Investigation of entrainment of sericite during presence and absence of hydrophobic microcrystalline graphite. • Entrained sericite had high impact on microcrystalline

	and Ying Lu		graphite during batch formation test.
Decrease of carbon dioxide concentration and entrainment of horizontally spreading ceiling jet	Yasushi Oka, Jun-ichi Yamaguchi and Ko Muraoka	Fire Safety Journal, Volume 63, January 2014, pp. 37-42.	• Objective of this paper is to find the information on the entrainment properties of ceiling jet spread radially. • An empirical formula was deduced. • Mass flow rate of ceiling jet increase with ceiling height.
Experimental study on unstable free surface vortices and gas entrainment onset conditions	Luca Cristofano, Matteo Nobili, Gianfranco Caruso	Experimental Thermal and Fluid Science, volume 52, January 2014, pp. 221-229	• GETS (gas entrainment test section) facility is built up and different experiment is carried out to study free surface vortices. • Parameters influencing the physical phenomenon is identified.
Liquid entrainment behavior at the nozzle exit in coaxial gas-liquid jets	Xiu-Sahn Tian, Hui zhao, Hai-Feng Liu, Wei-Feng Li and Jian-Liang Xu	Chemical Engineering Science, Volume 107, April 2014, pp. 93-101	• Experimental study on air-blast liquid jet and near-field recirculating behavior is conducted. • Formation of bulge structure when the gas velocity is larger than selected value. • Examination of transition of flow behavior. • Initial entrainment and full entrainment is observed and identified.

Visualization of air entrainment by plunging jet	A.K. Roy, B. Maiti and P.K. Das	Procedia Engineering, volume 56, 2013, pp. 468-473	• Formation of air-sheath below the interface shows the starting of entrainment. • Air sheath breaks into bubble, migrate downward and grow bigger due to coalescence. • Bigger bubble escape through free surface due to upward movement of it.
A model for droplet entrainment in churn flow	Ke Wang, Bofeng Bai and Weimin Ma	Chemical Engineering Science Volume 104, December 2013, pp. 1045-1055	• In churn flow, establishment of a mathematical model for droplet entrainment. • Analysis of the interface stability on the Kelvin–Helmholtz instability basis. • The proposed model is verified for a range of experimental data. • The influence of parameters on entrainment is discussed. • A formula for rate of entrainment in churn flow is proposed.
Huge wave and drop entrainment mechanism in gas-liquid churn flow	Ke Wang, Bofeng Bai and Weimin Ma	Chemical Engineering Science, Volume 104, December 2013, pp. 638-646	• In churn flow, huge wave and liquid distribution is investigated. • Discussion of situations for transition from churn flow to annular flow or slug flow. • Flooding is taken as a characteristic of churn flow.

			• Generation of drops due to bag breakup and ligament breakup mechanism in churn flow.
CFD Modelling of gas entrainment in stirred tank systems	A.L. Kulkarni and A.W Patwardhan	Chemical Engineering Research and Design, October 2013	• To study phenomenon of gas entrainment, CFD model is used. • Predicted velocity in impeller and interfacial region shows same velocity as in experiment. • Onset and non-onset condition was distinguished in CFD.
Computational study of crevice soot entrainment in a diesel engine	Shin Mei Tan, Hoon Kiat Ng, and Suyin Gan	Applied Energy, vol. 102, year. 2013, pp. 898-907	• Determination of parameters-effect on soot mass entrainment. • Compared to entrainment via blowby, formation of soot in crevice is insignificant. • Near cylinder liner, Soot is found higher than in the crevice region. • Soot entrainment is reduced by close-coupled injection. • Soot entrainment is increased to the greatest level due to delayed and split injection with large separation.
Numerical simulations of air entrainment in a plunging jet of liquid	Denis Brouilliot and Pierre Lubin	Journal of Fluids and Structures, Volume 43, November 2013, pp. 428-440	• Development of numerical model for classical VOF-PLIC model. • Compared to experimental data, this model give satisfactory results. • LES turbulence model is used. • VOF-SM is under development.

The origin of fine drops in batch gas-agitated liquid-liquid systems	Shahrokhi, H., & Shaw, J.M.	Chemical Engineering Science, Vol. 49, 5203-5213 (1994)	• Investigation of origin of drop. • Liquid entrainment as a principle source was found. • Criteria for the formation of fine drop was minimized.
Bubble induced entrainment between stratified liquid layers	Greene, G.A., Chen, J.C. & Conlin, M.T.	Int. J. Heat Mass Transfer, Vol. 34, 149-157 (1991)	• An analytical model is developed which shows the entrainment of liquid. • Entrainment efficiency is also calculated. • Experimental data is used to develop this model.
Onset of entrainment between immiscible liquid layers due to rising gas bubbles	Greene, G.A., Chen, J.C. & Conlin, M.T.	Int. J. Heat Mass Transfer, Vol. 31, 1309-1317 (1988)	• Inertial entrainment strength was obtained by measuring the volume of entrained liquid. • Different liquid pairs were used. • Experiment was carried to find minimum bubble volume to cause entrainment.

1.3 Gaps in the Literature

It can be seen from the literature review that there is a dearth of knowledge for three phase (liquid-liquid-gas) inertial entrainment. Also, there has been no attempt yet to simulate the three phase inertial entrainment. The strength of entrainment has been previously estimated by measuring the volume of entrained fluid. However, it does not take into account the height up to which the entrained fluid travels. The previous works on three phase entrainment also lay more emphasis on the penetration criteria. Hence, it

is clear that more investigation is required in the area of three phase inertial entrainment both experimentally as well as numerically.

1.4 Aims and Objectives

The present work aims to investigate the inertial entrainment phenomenon in three phase system (gas-liquid-liquid). The different objectives of this work are listed as follows:

- To study experimentally the phenomenon of three phase entrainment induced by a gas bubble in a stratified liquid layer.
- To quantify the strength of entrainment in terms of height achieved by the entrained volume.
- To identify different parameters that effect the phenomenon of entrainment.
- To observe and discuss the effect of fluid properties such as density, viscosity and surface tension, bubble volume and conduit wall proximity on the height of entrainment.
- To identify various stages that occur in inertial entrainment.
- To numerically simulate the phenomenon and check for the correlation between numerical and experimental results.

2 PROBLEM STATEMENT

The schematic of the problem statement is shown in **Figure 2.1**. It consists of a stratified layer of liquid. This stratified layer has two liquids- fluid 1 and fluid 2. Due to density difference and immiscibility, the fluid 1 and fluid 2 form the stratified layer with an interface. A gas bubble (fluid 3) is released in the lower liquid (fluid 1). The gas bubble tries to rise upwards because of buoyancy. As it moves upwards, it reaches the interface and tries to cross over to the upper liquid (fluid 2). When it crosses over, the bubble tries to take fluid 1 with it into fluid 2. However, the fluid 1 which is being pulled by the fluid 2, tends to remain attached with the bulk of fluid 1. A part of fluid 1 may break off from the bulk, and travel with the bubble upwards in fluid 2. After some duration, this part of fluid 1 travelling with bubble reaches a maximum height, then gets detached from the bubble. Now, it starts falling back and rejoins the bulk (fluid 1). This process of drawing in of one fluid into another is called entrainment. The output that we are interested in is the strength of such entrainment and the parameters that affect it. Different stages of entrainment are to be observed.

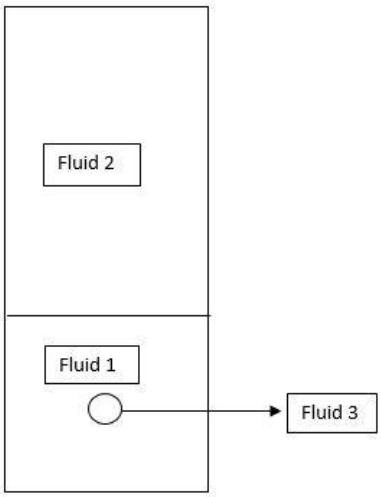

Figure 2.1 : Schematic of problem statement

3 METHODOLOGY

In this chapter, the methodology to tackle the problem have been discussed. The given problem can be solved in different ways. Here, experimental and numerical methods have been used to deduce useful data. Experiments have been conducted for a range of

parameters and numerical simulation has been shown for a particular parameter set. To measure the strength of entrainment, the maximum height attained by the fluid 1 is taken as an indicator (output).

3.1 Experiment

Many different methods can be adopted while conducting experiment to study a certain physical phenomenon. The methodology adopted here to carry our experiment is given below.

3.1.1 Setup

The schematic of the setup is shown alongside in **Figure 3.1**. The conduit is made of square cross section. The material is Perspex, also called acrylic resin. The sheets are joined using chloroform and powdered Perspex. The conduit is made leak proof by using Araldite. A syringe is fitted in the lower part of the conduit. This is used to inject the gas (fluid 3) to make the bubble. Since the syringe is capable of giving only small non-uniform bubbles with undesired volume, a bubble holding arrangement is also provided. This ensures that the bubble being released is of uniform size and required volume. The bubble holding arrangement consists of a piston. A hemispherical plastic cap is attached to this piston by means of a metal wire. The piston is used to exactly place the bubble at the centre of the

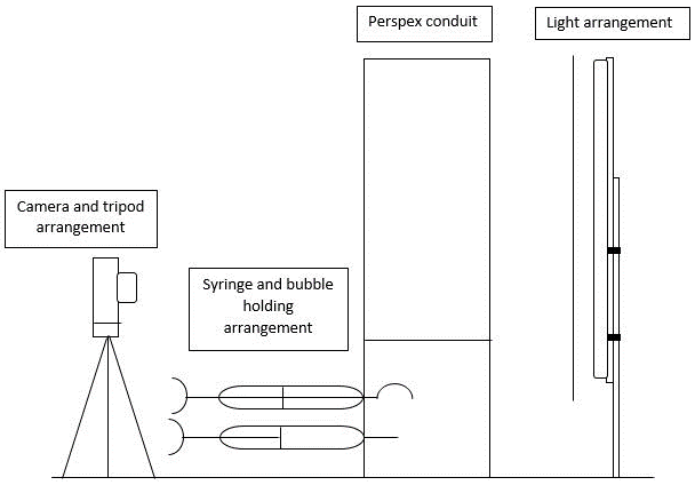

Figure 3.1: Schematic of experimental setup

conduit. The fluid 1 is filled in such a manner that the bubble holding arrangement occurs at exact midway of this fluid. The fluid 2 is filled above this layer of fluid 1. To record the phenomenon, a camera (mounted on a tripod) is placed in front of the setup. The camera height can be adjusted according to the requirement by use of the tripod. Behind the setup, a fluorescent tube lamp is provided to enable the camera to capture the interfaces clearly. Since diffused light is required, a sheet of butter paper is kept in front of the tube lamp. Also, for visibility, the water is colored green using dye. Kerosene is decolorized for the same reason.

Specification of the setup:

- Thickness of Perspex sheet: 5 mm
- Conduit cross-section: square of various dimensions
- Camera specification: 16MP Fujifilm S6800
- Video resolution: 1280p × 720p @ 30fps
- Light source: 40W @ 50 Hz

3.1.2 Parameters

Different parameters have been varied to study their effect on the strength of entrainment. The various parameters that have been considered here are fluid property parameters (density, viscosity, surface tension, and interfacial tension), wall effect (conduit dimensions) and bubble size (volume of fluid 3 in bubble). The fluid properties are varied by using three different pairs of fluid: kerosene-water, diesel-water, and petrol-water. The wall effect is studied by varying the conduit dimensions. Three dimensions taken were: 70 mm × 70 mm, 110 mm × 110 mm and 150 mm × 150 mm. The bubble sizes were varied from the minimum to maximum possible in the given

setup. This range depends on both the conduit dimension and fluid pair being used. The material properties are listed in **Table *3.1***.

Table 3.1: Material properties

Fluids	**Density (kg/m^3)**	**Viscosity (cP)**	**Interfacial tension (with water) (dynes/cm)**
Water	1000.00	1.0	N/A
Kerosene	817.15	2.1	48
Petrol	737.22	0.6	10^{-4} to 10^{-5}
Diesel	820.00	76.2	29

3.1.3 Working

For the experimental runs to be carried out, the light arrangement is switched on. The fluid 1 is filled first up to required level (300 mm). Then fluid 2 is filled over fluid 1 carefully to avoid mixing. The stratified layer is allowed to settle down and the interface is formed clearly. Now, the camera arrangement is set to capture the required area. To know the required arrangement, a test run is made as follows. The bubble of required volume is injected by one person from the lower syringe. The small bubbles are allowed to form a single bubble in the bubble holding arrangement placed just above the lower syringe. After the settling process, the upper syringe (piston arrangement) which is attached to the bubble holding mechanism is pushed to centre. This piston arrangement is then turned by the first person to release the bubble. At the same time the second person starts the recording of the camera to capture the whole phenomenon. Any required zoom adjustments is made by the second person. This first run is done as a test run to set the zoom levels, camera position and height correctly. After this, the

experimental runs are made as above, but now with the already set camera arrangement. The second person takes care of the video recording duration while the first person has the responsibility of releasing the bubble at the centre. The recording is done for the whole process, i.e., till the detached volume reaches its maximum height and then falls back to the original bulk of fluid 1.

To conduct different sets of experiments, the bubble volume is varied for a given combination of conduit size and fluid pair. The range of bubble size depends on these two itself and varies accordingly. For each combination of conduit size, fluid pair and bubble volume, five experimental runs are made. The arithmetic average of the five is taken as the accepted output.

3.1.4 Post-processing

The recorded videos are in .MP4 format. The image extraction is required for height measurement. It is not possible to extract frame by frame images from MP4 format files. Hence, the first step is conversion of MP4 format to AVI format. This conversion is done by means of an encoder-decoder called FFMPEG. FFMPEG is a command line based conversion tool. Now, the converted video has to split into frames. To do this, another software VirtualDub is used. This software takes AVI files as input and allows video frame by frame manipulation. The frame containing the fluid 1 reaching its maximum height is extracted manually using VirtualDub. Now, this frame is imported into GIMP (GNU Image Manipulation Program). This is done to measure the maximum height reached by fluid 1. The height is measured in pixels by using the Measure tool. To convert the height into physical measurement, we need a reference. The width of the conduit is known in physical measurement. Hence, the width is also measured in pixels. These two data are then input into an MS Excel workbook. The physical measurement of height is calculated by **Equation *3.1***.

$$\frac{Height\ in\ mm}{Width\ in\ mm} = \frac{Height\ in\ pixel}{Width\ in\ pixel}$$

Equation 3.1: Conversion of height in pixels to height in mm

The only unknown is height in mm. Thus, height is calculated.

3.2 Numerical

Numerical method has been used to simulate the phenomenon of inertial entrainment. The commercial solver ANSYS has been used for the same. Simulations have been carried out for both 2-dimensional and 3-dimensional cases.

3.2.1 Grid

The grid has been generated in ANSYS workbench. The grid for 2-dimensional case consists of 63000 cells while the grid for 3-dimensional case consists of 125000 cells. Both grids have been made on a mapped scheme.

3.2.2 Boundary conditions

The boundary conditions for the 2-dimensional case includes giving the left wall, right wall and bottom base as WALL, while the top edge is given the PRESSURE OUTLET condition. The boundary condition for 3-dimensional case follows the same: the four side walls and the bottom base are given WALL condition, while the top face is given the PRESSURE OUTLET condition. At the pressure outlet, the turbulence parameters are given as intensity and hydraulic diameter, with intensity set to 5%.

3.2.3 Governing equations

The governing equations that are solved in ANSYS are continuity (**Equation *3.2***), momentum (**Equation *3.3***) and volume fraction (**Equation *3.4***) equations. Since VOF model is used, the momentum equation is the same for all the phases, and a weighted average is used for the properties.

$$\nabla.(\rho\vec{v}) = 0$$

Equation 3.2: Continuity equation

$$\frac{\partial}{\partial t}(\rho\vec{v}) + \nabla.(\rho\vec{v}\vec{v}) = -\nabla p + \nabla.[\mu(\nabla\vec{v} + \nabla\vec{v}^T)] + \rho\vec{g}$$

Equation 3.3: Momentum equation

$$\frac{1}{\rho_q}[\frac{\partial}{\partial t}(\alpha_q\rho_q) + \nabla.(\alpha_q\rho_q\vec{v}_q) = \sum_{p=1}^{n}(\dot{m}_{pq} - \dot{m}_{qp})$$

Equation 3.4: Volume fraction equation

3.2.4 Solution method

Transient solution is attempted. The pressure based solver is used. For turbulence, standard k-ε model has been applied. Multiphase model has been enabled by using Volume of Fluid method with three phases. The primary phase is allotted as fluid 1, while secondary phases are fluid 2 and fluid 3. The bubble of fluid 3 and layer of fluid 2 are assigned before solving by patching respectively. The pressure-velocity coupling is done by the PISO scheme. The spatial discretization are done as follows: Green-Gauss cell based for Gradient, PRESTO for Pressure, Geo-Reconstruct for Volume Fraction, and First Order Upwind for Momentum, Turbulent Kinetic Energy and Turbulent Dissipation Energy. The transient formulation is first order implicit. The convergence criteria for all of the variables (continuity, velocities, k and ε) are set as 1e-6. The maximum number of iterations allowed per time step is set as 50. The time step has been given as 0.0001s, auto-saving every 50 time steps.

4 RESULTS AND DISCUSSION

This section is devoted to representation of the results obtained (both from experimental and numerical approaches) and list probable causes for the variations observed.

4.1 Individual combinations of conduit dimension and fluid pair

For a given combination of conduit dimension and fluid pair, experimental runs were conducted by varying the bubble volume. The data obtained and its graphical representation for each combination is given below. The first table in each sub-division shows the detailed calculation as well as observation of 5 runs for a particular bubble volume. The arithmetic average height thus obtained from the 5 data is shown in the next column of the same table. The second table in each sub-division shows the filtered data (only bubble volume and average height of entrainment) in SI units. This is followed by the graph of height of entrainment versus bubble volume. The discussions are noted at the end of each sub-division.

4.1.1 Conduit Dimension: 70 mm × 70 mm

The detailed results obtained for conduit dimension 70 mm × 70 mm is shown below for each fluid pair.

4.1.1.1 Fluid pair: Kerosene-Water

The detailed observation for each experimental run is given in **Table *4.1***.

Table 4.1: Detailed observation for experimental runs of conduit dimension 70 mm x 70 mm and fluid pair kerosene-water

Bubble volume in ml	Run No.	Width in px	Height in px	Width in mm	Height in mm	Average Height in mm
0.5	1	190	201	80	84.63157895	84.29473684
	2	190	195	80	82.10526316	
	3	190	198	80	83.36842105	
	4	190	200	80	84.21052632	
	5	190	207	80	87.15789474	
0.6	1	169	224	80	106.0355030	123.9410623
	2	168	303	80	144.2857143	
	3	174	258	80	118.6206897	
	4	173	244	80	112.8323699	
	5	174	300	80	137.9310345	
0.7	1	171	212	80	99.18128655	167.6469286

	2	166	416	80	200.4819277	
	3	168	406	80	193.3333333	
	4	168	361	80	171.9047619	
	5	168	364	80	173.3333333	
0.8	1	167	319	80	152.8143713	181.2119887
	2	169	500	80	236.6863905	
	3	170	375	80	176.4705882	
	4	172	379	80	176.2790698	
	5	168	344	80	163.8095238	
0.9	1	190	377	80	158.7368421	190.837033
	2	189	486	80	205.7142857	
	3	195	391	80	160.4102564	
	4	191	450	80	188.4816754	
	5	190	572	80	240.8421053	
1	1	190	427	80	179.7894737	217.8004503
	2	186	314	80	135.0537634	
	3	190	613	80	258.1052632	
	4	190	881	80	370.9473684	
	5	188	341	80	145.1063830	
1.1	1	186	549	80	236.1290323	230.4221456
	2	188	733	80	311.9148936	
	3	188	442	80	188.0851064	
	4	185	590	80	255.1351351	
	5	189	380	80	160.8465608	
1.2	1	204	540	80	211.7647059	214.9422494
	2	204	694	80	272.1568627	
	3	205	505	80	197.0731707	
	4	207	528	80	204.0579710	
	5	205	486	80	189.6585366	
1.3	1	202	538	80	213.0693069	273.0915837
	2	202	634	80	251.0891089	
	3	200	1103	80	441.2000000	
	4	201	713	80	283.7810945	
	5	201	443	80	176.3184080	
1.4	1	201	688	80	273.8308458	288.4920469
	2	201	816	80	324.7761194	
	3	201	813	80	323.5820896	
	4	202	644	80	255.0495050	
	5	203	673	80	265.2216749	
1.5	1	203	914	80	360.1970443	311.3705379
	2	203	799	80	314.8768473	
	3	213	714	80	268.1690141	
	4	201	908	80	361.3930348	
	5	203	640	80	252.2167488	

1.6	1	175	700	80	320.0000000	334.6342906
	2	166	560	80	269.8795181	
	3	164	618	80	301.4634146	
	4	163	611	80	299.8773006	
	5	164	988	80	481.9512195	
1.7	1	159	581	80	292.3270440	364.5225682
	2	159	800	80	402.5157233	
	3	176	1078	80	490.0000000	
	4	171	712	80	333.0994152	
	5	167	636	80	304.6706587	

The average of the five runs per bubble volume is taken as the output. The bubble volume with average height of entrainment in SI units is given in **Table *4.2***.

Table 4.2: Average height of entrainment for conduit dimension 70 mm × 70 mm and fluid pair kerosene-water

Bubble volume in m^3	Height of entrainment in m
5.00E-07	0.084294737
6.00E-07	0.123941062
7.00E-07	0.167646929
8.00E-07	0.181211989
9.00E-07	0.190837033
1.00E-06	0.217800450
1.10E-06	0.230422146
1.20E-06	0.214942249
1.30E-06	0.273091584
1.40E-06	0.288492047
1.50E-06	0.311370538
1.60E-06	0.334634291
1.70E-06	0.364522568

The graph for observing the trend is plot from the data in **Table *4.2*** and the plot is shown in **Graph *4.1***.

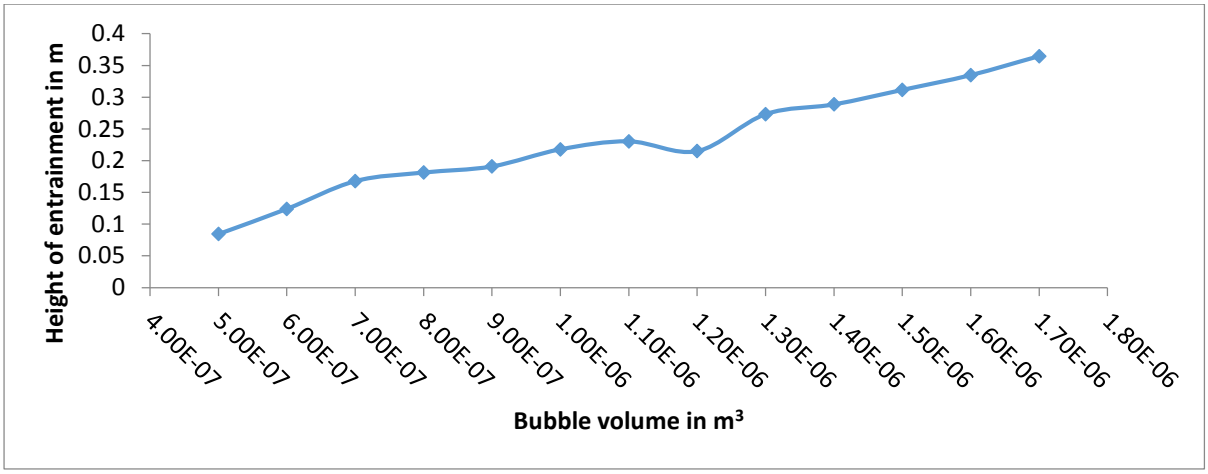

Graph 4.1: Graph for height of entrainment versus bubble volume for conduit dimension 70 mm × 70 mm and fluid pair kerosene-water

The trend observed from the above graph is clear. As the bubble volume increases, the height of entrainment increases almost linearly. There is a slight dip at bubble volume 1.2 ml. This may be attributed to random error.

4.1.1.2 Fluid pair: Diesel-Water

The detailed observation for each experimental run is given in **Table *4.3***.

Table 4.3: Detailed observation for experimental runs of conduit dimension 70 mm × 70 mm and fluid pair diesel-water

Bubble volume in ml	Run No.	Width in px	Height in px	Width in mm	Height in mm	Average Height in mm
0.6	1	140	189	80	108.0000000	105.8824545
	2	141	217	80	123.1205674	
	3	138	172	80	99.7101449	
	4	141	144	80	81.7021276	
	5	141	206	80	116.8794326	
0.7	1	143	210	80	117.4825175	129.086178
	2	140	204	80	116.5714286	
	3	140	199	80	113.7142857	
	4	141	213	80	120.8510638	
	5	138	305	80	176.8115942	
0.8	1	142	226	80	127.3239437	142.317216
	2	136	326	80	191.7647059	
	3	139	181	80	104.1726619	
	4	140	285	80	162.8571429	

	5	139	218	80	125.4676259	
0.9	1	138	306	80	177.3913043	157.2046969
	2	137	209	80	122.0437956	
	3	137	324	80	189.1970803	
	4	138	300	80	173.9130435	
	5	138	213	80	123.4782609	
1	1	139	332	80	191.0791367	182.5129154
	2	140	292	80	166.8571429	
	3	139	315	80	181.2949640	
	4	138	303	80	175.6521739	
	5	138	341	80	197.6811594	
1.1	1	137	430	80	251.0948905	211.9422732
	2	139	374	80	215.2517986	
	3	133	374	80	224.9624060	
	4	137	296	80	172.8467153	
	5	135	330	80	195.5555556	
1.2	1	135	320	80	189.6296296	224.2513886
	2	137	302	80	176.3503650	
	3	135	393	80	232.8888889	
	4	134	307	80	183.2835821	
	5	134	568	80	339.1044776	
1.3	1	138	364	80	211.0144928	228.7542949
	2	136	393	80	231.1764706	
	3	138	419	80	242.8985507	
	4	137	397	80	231.8248175	
	5	140	397	80	226.8571429	
1.4	1	133	462	80	277.8947368	299.0265515
	2	133	612	80	368.1203008	
	3	135	486	80	288.0000000	
	4	133	515	80	309.7744361	
	5	134	421	80	251.3432836	
1.5	1	135	334	80	197.9259259	317.7980241
	2	133	808	80	486.0150376	
	3	135	427	80	253.0370370	
	4	133	548	80	329.6240602	
	5	134	540	80	322.3880597	
1.6	1	134	535	80	319.4029851	334.663726
	2	135	631	80	373.9259259	
	3	134	508	80	303.2835821	
	4	135	598	80	354.3703704	
	5	137	552	80	322.3357664	

The average of the five runs per bubble volume is taken as the output. The bubble volume with average height of entrainment in SI units is given in **Table *4.4***.

Table 4.4: Average height of entrainment for conduit dimension 70 mm × 70 mm and fluid pair diesel-water

Bubble volume in m^3	Height of entrainment in m
6.00E-07	0.105882455
7.00E-07	0.129086178
8.00E-07	0.142317216
9.00E-07	0.157204697
1.00E-06	0.182512915
1.10E-06	0.211942273
1.20E-06	0.224251389
1.30E-06	0.228754295
1.40E-06	0.299026551
1.50E-06	0.317798024
1.60E-06	0.334663726

The graph for observing the trend is plot from the data in **Table *4.4*** and the plot is shown in **Graph *4.2***.

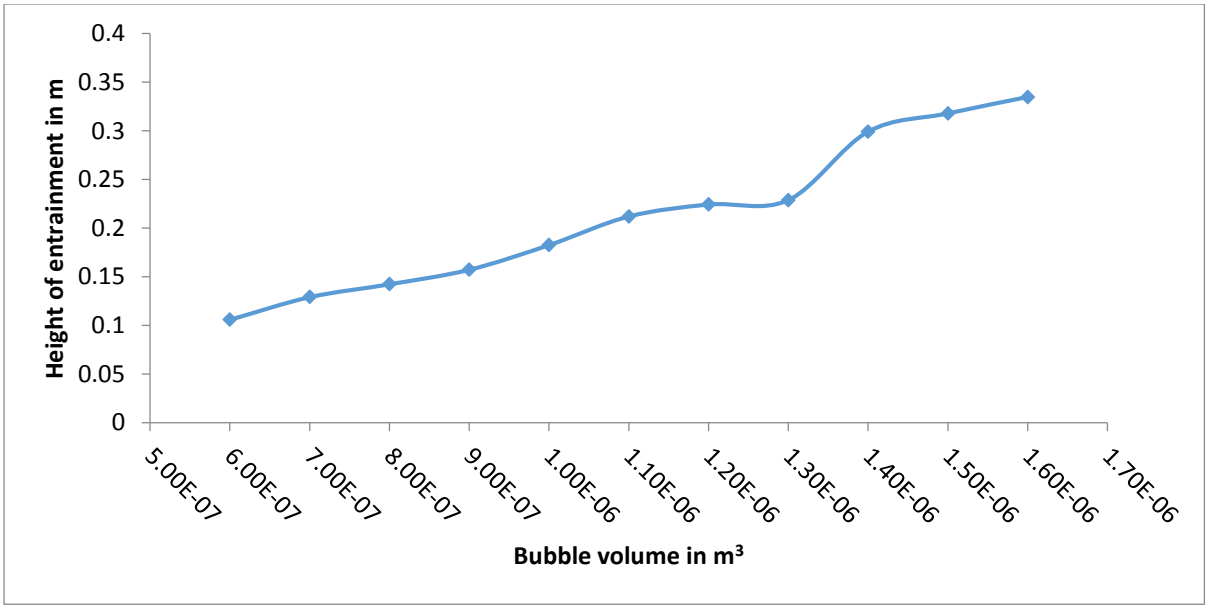

Graph 4.2: **Graph for height of entrainment versus bubble volume for conduit dimension 70 mm × 70 mm and fluid pair diesel-water**

The trend observed from the above graph is that the height of entrainment increases as bubble volume increases. The dip at 1.3 ml may be due to random error as the dip is very less.

4.1.1.3 Fluid pair: Petrol-water

The detailed observation for experimental run is given in **Table *4.5***.

Table 4.5: Detailed observation for experimental runs of conduit dimension 70 mm × 70 mm and fluid pair petrol-water

Bubble volume in ml	Run No.	Width in px	Height in px	Width in mm	Height in mm	Average Height in mm
1	1	138	692	80	401.1594203	387.8386344
	2	144	768	80	426.6666667	
	3	139	633	80	364.3165468	
	4	136	771	80	453.5294118	
	5	142	521	80	293.5211268	
1.1	1	138	614	80	355.9420290	311.9673994
	2	141	492	80	279.1489362	
	3	144	529	80	293.8888889	
	4	140	483	80	276.0000000	
	5	140	621	80	354.8571429	
1.2	1	143	371	80	207.5524476	241.7016252
	2	147	489	80	266.1224490	
	3	139	374	80	215.2517986	
	4	146	566	80	310.1369863	
	5	144	377	80	209.4444444	
1.3	1	148	593	80	320.5405405	285.6707072
	2	144	577	80	320.5555556	
	3	146	452	80	247.6712329	
	4	145	398	80	219.5862069	
	5	139	556	80	320.0000000	
1.4	1	139	420	80	241.7266187	261.5204341
	2	144	600	80	333.3333333	
	3	143	369	80	206.4335664	
	4	140	479	80	273.7142857	
	5	142	448	80	252.3943662	
1.5	1	147	579	80	315.1020408	253.6490339
	2	144	439	80	243.8888889	
	3	145	373	80	205.7931034	
	4	152	565	80	297.3684211	

	5	151	389	80	206.0927152	
1.6	1	148	423	80	228.6486486	258.3636045
	2	145	538	80	296.8275862	
	3	157	521	80	265.4777070	
	4	151	478	80	253.2450331	
	5	147	455	80	247.6190476	
1.7	1	140	555	80	317.1428571	280.1230585
	2	131	440	80	268.7022901	
	3	138	659	80	382.0289855	
	4	141	460	80	260.9929078	
	5	143	307	80	171.7482517	

The average of the five runs per bubble volume is taken as the output. The bubble volume with average height of entrainment in SI units is given in **Table *4.6***.

Table 4.6: Average height of entrainment for conduit dimension 70 mm × 70 mm and fluid pair petrol-water

Bubble volume in m^3	Height of entrainment in m
1.00E-06	0.387838634
1.10E-06	0.311967399
1.20E-06	0.241701625
1.30E-06	0.285670707
1.40E-06	0.261520434
1.50E-06	0.253649034
1.60E-06	0.258363605
1.70E-06	0.280123058

The graph for observing the trend is plot from the data in **Table *4.6*** and the plot is shown in **Graph *4.3***.

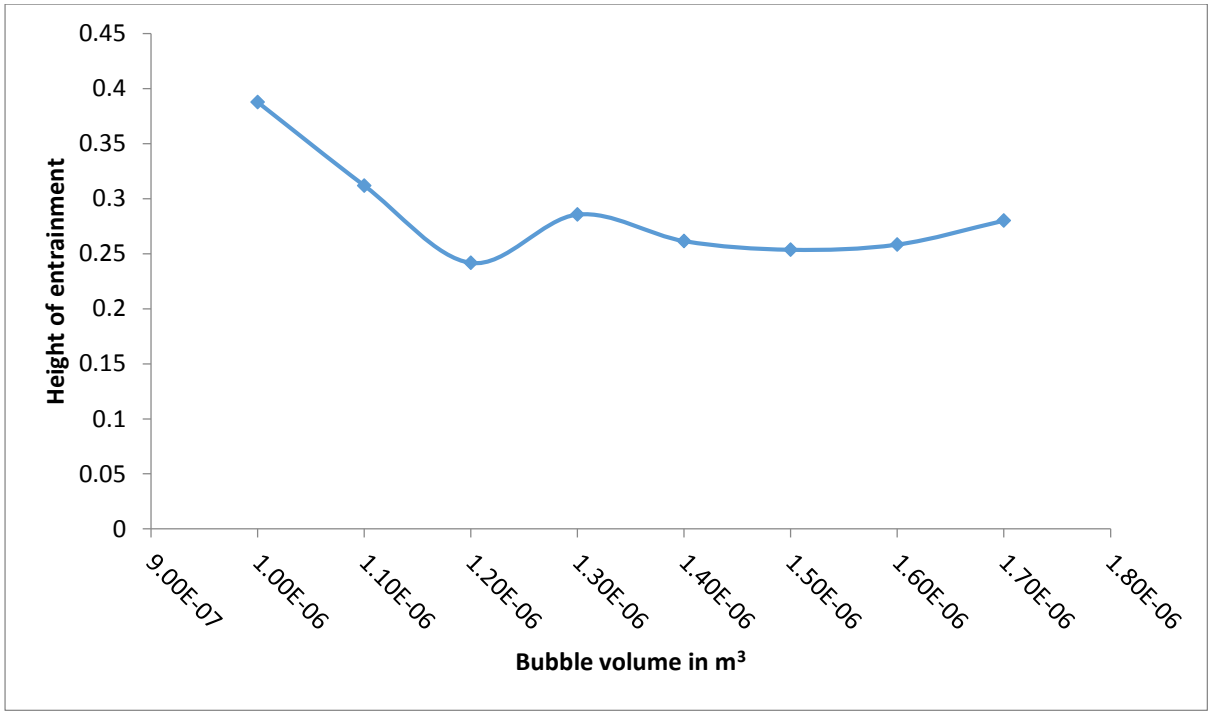

Graph 4.3: Graph for height of entrainment versus bubble volume for conduit dimension 70 mm × 70 mm and fluid pair petrol-water

Petrol shows a unique behavior. The height first decreases, reaches a minimum and then starts to increase slowly. The initial decrease is rapid, while the increase that occurs later is slow and gradual.

4.1.2 Conduit dimension: 110 mm × 110 mm

The detailed results obtained for conduit dimension 110 mm × 110 mm is shown below for each fluid pair.

4.1.2.1 Fluid pair: Kerosene-water

The detailed observation for experimental run is given in **Table *4.7***.

Table 4.7: Detailed observation for experimental runs of conduit dimension 110 mm × 110 mm and fluid pair kerosene-water

Bubble volume in ml	Run No.	Width in px	Height in px	Width in mm	Height in mm	Average Height in mm
0.6	1	356	284	120	95.73033708	115.7690433
	2	342	356	120	124.9122807	
	3	331	340	120	123.2628399	
	4	332	310	120	112.0481928	
	5	332	340	120	122.8915663	
0.7	1	322	361	120	134.5341615	136.3380157
	2	325	420	120	155.0769231	
	3	312	324	120	124.6153846	
	4	340	389	120	137.2941176	
	5	295	320	120	130.1694915	
0.8	1	287	428	120	178.9547038	167.9744644
	2	306	466	120	182.7450980	
	3	305	296	120	116.4590164	
	4	308	333	120	129.7402597	
	5	299	578	120	231.9732441	
0.9	1	284	427	120	180.4225352	191.7110842
	2	274	419	120	183.5036496	
	3	295	503	120	204.6101695	
	4	294	453	120	184.8979592	
	5	289	494	120	205.1211073	
1	1	340	520	120	183.5294118	210.8058068
	2	335	513	120	183.7611940	
	3	334	694	120	249.3413174	
	4	356	668	120	225.1685393	
	5	350	619	120	212.2285714	
1.1	1	366	845	120	277.0491803	238.0253924
	2	356	666	120	224.4943820	
	3	358	569	120	190.7262570	
	4	336	726	120	259.2857143	
	5	336	668	120	238.5714286	
1.2	1	288	583	120	242.9166667	248.0316918
	2	321	662	120	247.4766355	
	3	288	516	120	215.0000000	
	4	287	550	120	229.9651568	
	5	300	762	120	304.8000000	
1.3	1	303	683	120	270.4950495	259.0225445
	2	302	665	120	264.2384106	
	3	310	623	120	241.1612903	
	4	301	584	120	232.8239203	

	5	269	642	120	286.3940520	
1.4	1	297	576	120	232.7272727	282.8188714
	2	279	652	120	280.4301075	
	3	233	702	120	361.5450644	
	4	276	512	120	222.6086957	
	5	286	755	120	316.7832168	
1.5	1	300	658	120	263.2000000	291.9386268
	2	276	731	120	317.8260870	
	3	286	634	120	266.0139860	
	4	306	918	120	360.0000000	
	5	294	619	120	252.6530612	

The average of the five runs per bubble volume is taken as the output. The bubble volume with average height of entrainment in SI units is given in **Table *4.8***.

Table 4.8: Average height of entrainment for conduit dimension 110 mm × 110 mm and fluid pair kerosene-water

Bubble volume in m^3	Height of entrainment in m
6.00E-07	0.115769043
7.00E-07	0.136338016
8.00E-07	0.167974464
9.00E-07	0.191711084
1.00E-06	0.210805807
1.10E-06	0.238025392
1.20E-06	0.248031692
1.30E-06	0.259022545
1.40E-06	0.282818871
1.50E-06	0.291938627

The graph for observing the trend is plot from the data in **Table *4.8*** and the plot is shown in **Graph *4.4***.

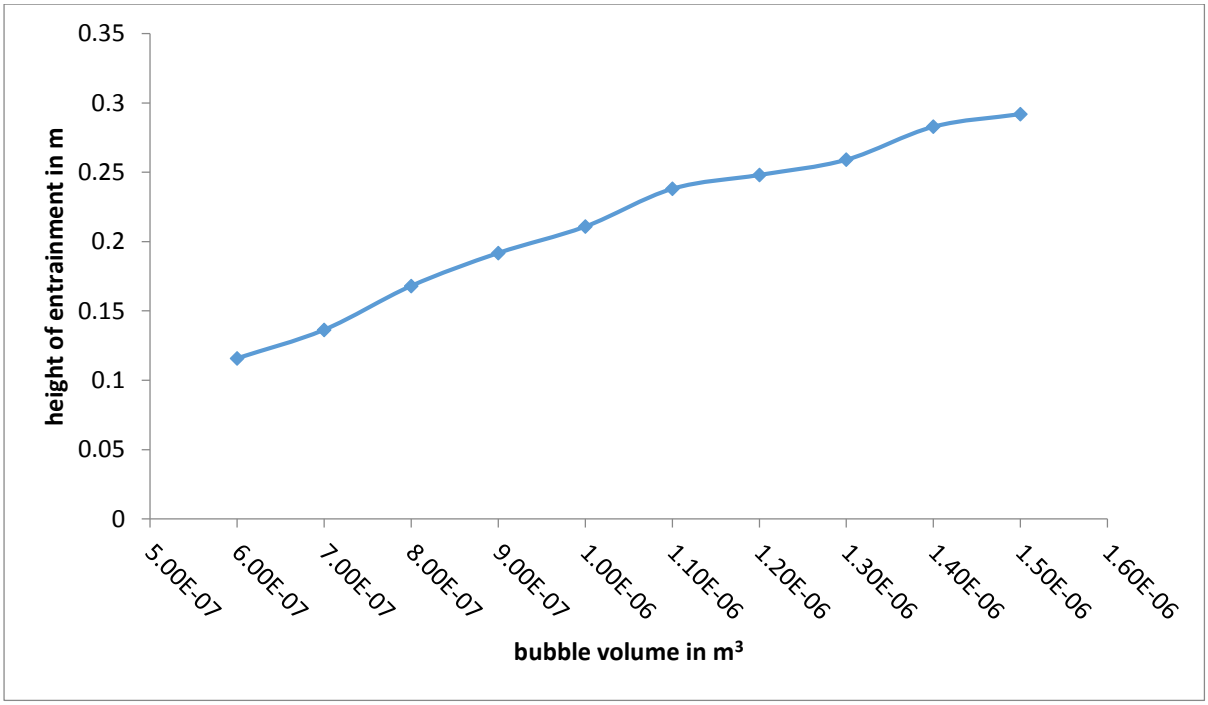

Graph 4.4: Graph for height of entrainment versus bubble volume for conduit dimension 110 mm × 110 mm and fluid pair kerosene-water

The trend is almost linear in nature. As bubble volume increases, the height of entrainment also increases.

4.1.2.2 Fluid pair: Diesel-water

The detailed observation for experimental run is given in **Table *4.9***.

Table 4.9: Detailed observation for experimental runs of conduit dimension 110 mm × 110 mm and fluid pair diesel-water

Bubble Volume	Run No.	Width in px	Height in px	Width in mm	Height in mm	Average Height in mm
0.5	1	416	823	110	217.6201923	214.4572893
	2	354	726	110	225.5932203	
	3	368	691	110	206.5489130	
	4	462	912	110	217.1428571	
	5	459	857	110	205.3812636	
0.6	1	470	929	110	217.4255319	234.0672143
	2	468	998	110	234.5726496	
	3	468	977	110	229.6367521	
	4	473	1090	110	253.4883721	
	5	470	1005	110	235.2127660	
0.7	1	376	873	110	255.3989362	243.0011

	2	323	660	110	224.7678019	
	3	376	912	110	266.8085106	
	4	398	666	110	184.0703518	
	5	399	1030	110	283.9598997	
0.8	1	408	684	110	184.4117647	219.612318
	2	418	1103	110	290.2631579	
	3	417	678	110	178.8489209	
	4	419	1155	110	303.2219570	
	5	418	537	110	141.3157895	
0.9	1	445	1119	110	276.6067416	263.2225873
	2	411	912	110	244.0875912	
	3	379	774	110	224.6437995	
	4	411	1131	110	302.7007299	
	5	405	987	110	268.0740741	
1	1	376	795	110	232.5797872	241.9094381
	2	412	962	110	256.8446602	
	3	352	751	110	234.6875000	
	4	411	770	110	206.0827251	
	5	417	1059	110	279.3525180	
1.1	1	349	822	110	259.0830946	292.0440632
	2	333	1007	110	332.6426426	
	3	371	983	110	291.4555256	
	4	343	915	110	293.4402332	
	5	339	874	110	283.5988201	
1.2	1	330	951	110	317.0000000	339.9637668
	2	304	876	110	316.9736842	
	3	304	855	110	309.3750000	
	4	309	1013	110	360.6148867	
	5	304	1094	110	395.8552632	

The average of the five runs per bubble volume is taken as the output. The bubble volume with average height of entrainment in SI units is given in **Table *4.10***.

Table 4.10: Average height of entrainment for conduit dimension 110 mm × 110 mm and fluid pair diesel-water

Bubble volume in m^3	Height of entrainment in m
5.00E-07	0.214457289
6.00E-07	0.234067214
7.00E-07	0.243001100
8.00E-07	0.219612318
9.00E-07	0.263222587

1.00E-06	0.241909438
1.10E-06	0.292044063
1.20E-06	0.339963767

The graph for observing the trend is plot from the data in **Table *4.10*** and the plot is shown in **Graph *4.5***.

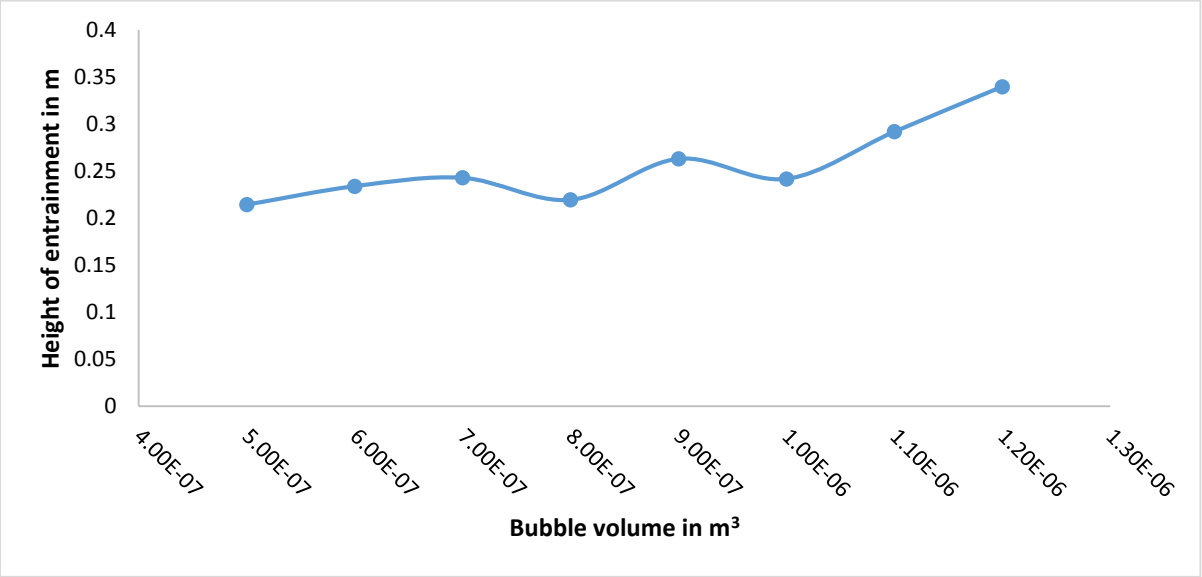

Graph 4.5: Graph for height of entrainment versus bubble volume for conduit dimension 110 mm × 110 mm and fluid pair diesel-water

The height of entrainment increases almost linearly with bubble volume. Slight dips are observed at bubble volumes 0.8ml and 1ml.

4.1.2.3 Fluid pair: Petrol-water

The detailed observation for experimental run is given in **Table *4.11***.

Table 4.11: Detailed observation for experimental runs of conduit dimension 110 mm × 110 mm and fluid pair petrol-water

Bubble Volume	Run No.	Width in px	Height in px	Width in mm	Height in mm	Average Height in mm
0.8	1	440	747	110	186.7500000	178.1371243
	2	408	616	110	166.0784314	
	3	371	593	110	175.8221024	
	4	405	702	110	190.6666667	

	5	380	592	110	171.3684211	
0.9	1	288	631	110	241.0069444	223.0146154
	2	298	672	110	248.0536913	
	3	294	440	110	164.6258503	
	4	293	638	110	239.5221843	
	5	295	595	110	221.8644068	

The average of the five runs per bubble volume is taken as the output. The bubble volume with average height of entrainment in SI units is given in **Table *4.12***.

Table 4.12: Average height of entrainment for conduit dimension 110 mm × 110 mm and fluid pair petrol-water

Bubble volume in m^3	Height of entrainment in m
8.00E-07	0.178137124
9.00E-07	0.223014615

The graph for observing the trend is plot from the data in **Table *4.12*** and the plot is shown in **Graph *4.6***.

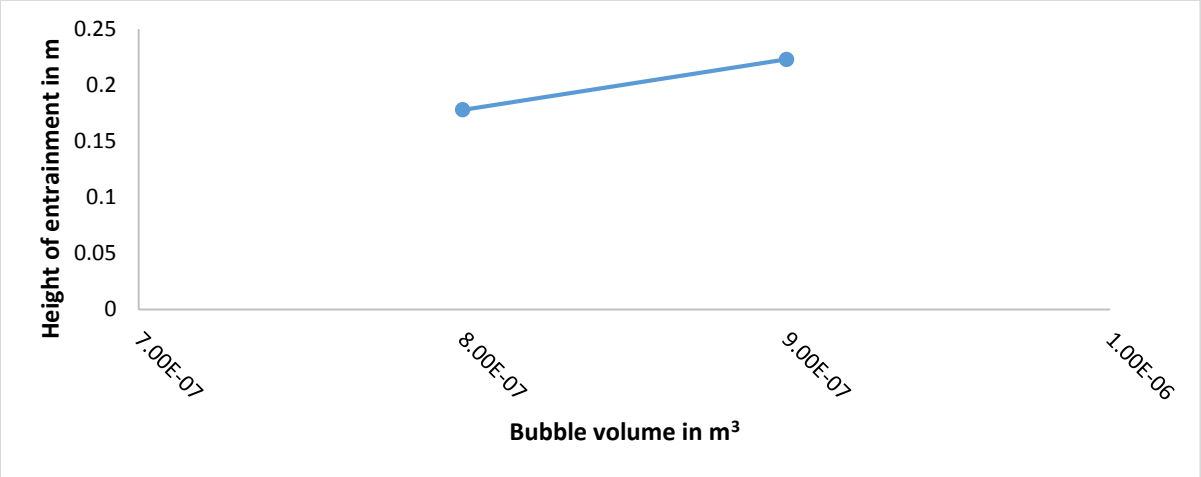

Graph 4.6: Graph for height of entrainment versus bubble volume for conduit dimension 110 mm × 110 mm and fluid pair petrol-water

Any trend cannot be established here. The range of bubble size allowed by the conduit here is too small to establish for certain any trend. However, the height of entrainment increases with bubble volume as observed from the two data points given above.

4.1.3 Conduit dimension: 150 mm × 150 mm

The detailed results obtained for conduit dimension 150 mm × 150 mm is shown below for the only fluid pair.

4.1.3.1 Fluid pair: Kerosene-water

The detailed observation for experimental run is given in **Table *4.13***.

Table 4.13: Detailed observation for experimental runs of conduit dimension 150 mm × 150 mm and fluid pair kerosene-water

Bubble Volume in ml	Run No.	Width in px	Height in px	Width in mm	Height in mm	Average height in mm
0.5	1	546	304	160	89.08424908	91.50799593
	2	475	318	160	107.1157895	
	3	474	279	160	94.17721519	
	4	526	279	160	84.86692015	
	5	453	233	160	82.29580574	
0.6	1	413	379	160	146.8280872	133.6268989
	2	414	332	160	128.3091787	
	3	413	312	160	120.8716707	
	4	415	327	160	126.0722892	
	5	413	377	160	146.0532688	
0.7	1	479	524	160	175.0313152	166.9765312
	2	474	463	160	156.2869198	
	3	476	490	160	164.7058824	
	4	456	478	160	167.7192982	
	5	474	507	160	171.1392405	
0.8	1	478	529	160	177.0711297	177.4673485
	2	477	550	160	184.4863732	
	3	38	587	10	154.4736842	
	4	40	703	10	175.7500000	
	5	36	704	10	195.5555556	
0.9	1	463	450	160	155.5075594	186.6236075

	2	465	698	160	240.1720430	
	3	463	564	160	194.9028078	
	4	464	584	160	201.3793103	
	5	467	412	160	141.1563169	
1	1	33	629	10	190.6060606	195.8450245
	2	549	719	160	209.5446266	
	3	543	654	160	192.7071823	
	4	553	712	160	206.0036166	
	5	550	620	160	180.3636364	
1.1	1	463	586	160	202.5053996	211.343262
	2	471	468	160	158.9808917	
	3	452	529	160	187.2566372	
	4	437	644	160	235.7894737	
	5	435	740	160	272.1839080	
1.2	1	477	688	160	230.7756813	221.8968242
	2	488	727	160	238.3606557	
	3	479	570	160	190.3966597	
	4	31	695	10	224.1935484	
	5	33	745	10	225.7575758	
1.3	1	430	591	160	219.9069767	221.3713352
	2	435	573	160	210.7586207	
	3	436	589	160	216.1467890	
	4	435	705	160	259.3103448	
	5	436	547	160	200.7339450	
1.4	1	562	854	160	243.1316726	231.7332423
	2	563	863	160	245.2575488	
	3	32	774	10	241.8750000	
	4	551	738	160	214.3012704	
	5	556	744	160	214.1007194	
1.5	1	431	758	160	281.3921114	256.5828411
	2	453	681	160	240.5298013	
	3	438	688	160	251.3242009	
	4	438	614	160	224.2922374	
	5	439	783	160	285.3758542	
1.6	1	489	697	160	228.0572597	260.7462271
	2	31	932	10	300.6451613	
	3	33	839	10	254.2424242	
	4	31	822	10	265.1612903	
	5	32	818	10	255.6250000	

The average of the five runs per bubble volume is taken as the output. The bubble volume with average height of entrainment in SI units is given in **Table *4.14***.

Table 4.14: Average height of entrainment for conduit dimension 150 mm × 150 mm and fluid pair kerosene-water

Bubble Volume in m^3	Height of entrainment in m
5.00E-07	0.091507996
6.00E-07	0.133626899
7.00E-07	0.166976531
8.00E-07	0.177467349
9.00E-07	0.186623607
1.00E-06	0.195845025
1.10E-06	0.211343262
1.20E-06	0.221896824
1.30E-06	0.221371335
1.40E-06	0.231733242
1.50E-06	0.256582841
1.60E-06	0.260746227

The graph for observing the trend is plot from the data in **Table *4.14*** and the plot is shown in **Graph *4.7***.

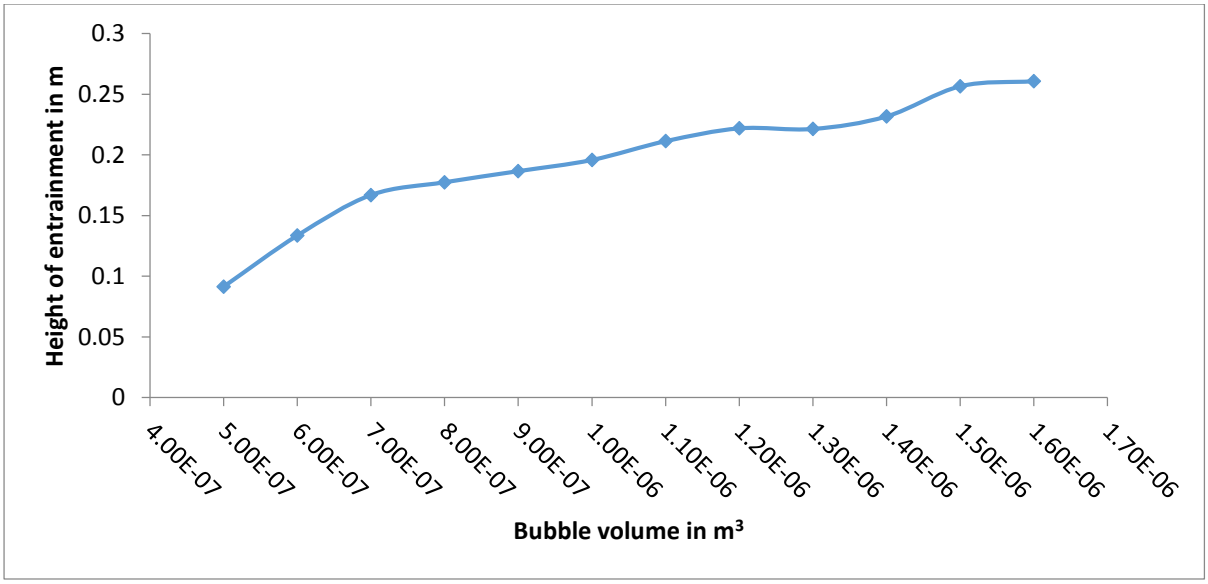

Graph 4.7: Graph for height of entrainment versus bubble volume for conduit dimension 150 mm × 150 mm and fluid pair kerosene-water

The trend is almost linear. As the bubble volume increases, the height of entrainment increases.

4.2 Effect of conduit dimension

The effect of conduit dimension has been studied by comparing the results for a single fluid pair (kerosene-water) in three different conduit dimensions. The data is given in **Table *4.15***. A graph is show below in **Graph *4.8***.

Table 4.15: Comparison of average height of entrainment for different conduit dimension with fluid pair kerosene-water

70 mm × 70 mm		**110 mm × 110 mm**		**150 mm × 150 mm**	
Bubble volume in m^3	**Height of entrainment in m**	**Bubble volume in m^3**	**Height of entrainment in m**	**Bubble Volume in m^3**	**Height of entrainment in m**
5.00E-07	0.084294737	6.00E-07	0.115769043	5.00E-07	0.091507996
6.00E-07	0.123941062	7.00E-07	0.136338016	6.00E-07	0.133626899
7.00E-07	0.167646929	8.00E-07	0.167974464	7.00E-07	0.166976531
8.00E-07	0.181211989	9.00E-07	0.191711084	8.00E-07	0.177467349
9.00E-07	0.190837033	1.00E-06	0.210805807	9.00E-07	0.186623607
1.00E-06	0.217800450	1.10E-06	0.238025392	1.00E-06	0.195845025
1.10E-06	0.230422146	1.20E-06	0.248031692	1.10E-06	0.211343262
1.20E-06	0.214942249	1.30E-06	0.259022545	1.20E-06	0.221896824
1.30E-06	0.273091584	1.40E-06	0.282818871	1.30E-06	0.221371335
1.40E-06	0.288492047	1.50E-06	0.291938627	1.40E-06	0.231733242
1.50E-06	0.311370538			1.50E-06	0.256582841
1.60E-06	0.334634291			1.60E-06	0.260746227
1.70E-06	0.364522568				

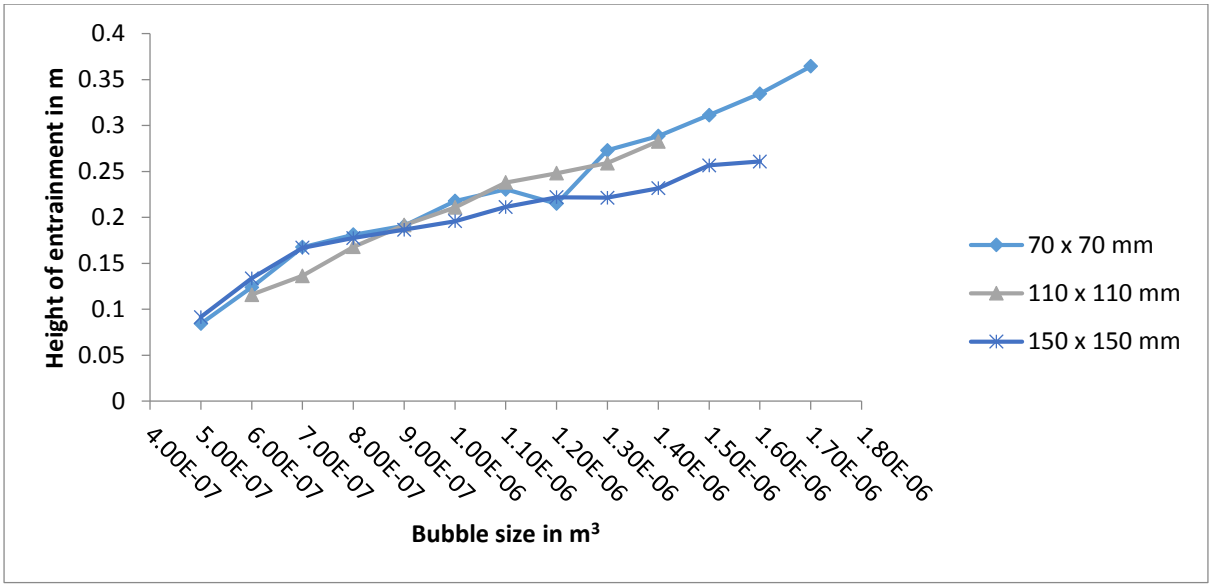

Graph 4.8: Graph showing the effect of conduit dimension for fluid pair kerosene-water

It can be observed from the graph that when the bubble volume is low (up to 0.8ml) the effect of conduit dimension is negligible. However, with increasing bubble volume, differences can be clearly observed between the heights attained by bubbles of a given volume in conduits of different dimension. The heights attained in conduit dimension 110 mm × 110 mm are the maximum of the three dimensions. The heights attained in conduit dimension 150 mm × 150 mm are the minimum of the three dimensions. The heights attained in conduit dimension 70 mm × 70 mm lie in between the other two.

4.3 Effect of fluid pair combination

The effect of fluid pair combination is studied by means of comparing the data for three different fluid pairs (kerosene-water, petrol-water and diesel-water) in a single conduit dimension (70 mm × 70 mm). The data used for comparison is given below in **Table *4.16***. The graph for the data given below is show in **Graph *4.9***.

Table 4.16: Comparison of average height of entrainment for different fluid pair for conduit dimension 70 mm × 70 mm

Kerosene		Petrol		Diesel	
Bubble volume in m^3	Height of entrainment in m	Bubble volume in m^3	Height of entrainment in m	Bubble volume in m^3	Height of entrainment in m
5.00E-07	0.084294737	1.00E-06	0.387838634	6.00E-07	0.105882455
6.00E-07	0.123941062	1.10E-06	0.311967399	7.00E-07	0.129086178
7.00E-07	0.167646929	1.20E-06	0.241701625	8.00E-07	0.142317216
8.00E-07	0.181211989	1.30E-06	0.285670707	9.00E-07	0.157204697
9.00E-07	0.190837033	1.40E-06	0.261520434	1.00E-06	0.182512915
1.00E-06	0.217800450	1.50E-06	0.253649034	1.10E-06	0.211942273
1.10E-06	0.230422146	1.60E-06	0.258363605	1.20E-06	0.224251389
1.20E-06	0.214942249	1.70E-06	0.280123058	1.30E-06	0.228754295
1.30E-06	0.273091584			1.40E-06	0.299026551
1.40E-06	0.288492047			1.50E-06	0.317798024
1.50E-06	0.311370538			1.60E-06	0.334663726
1.60E-06	0.334634291				
1.70E-06	0.364522568				

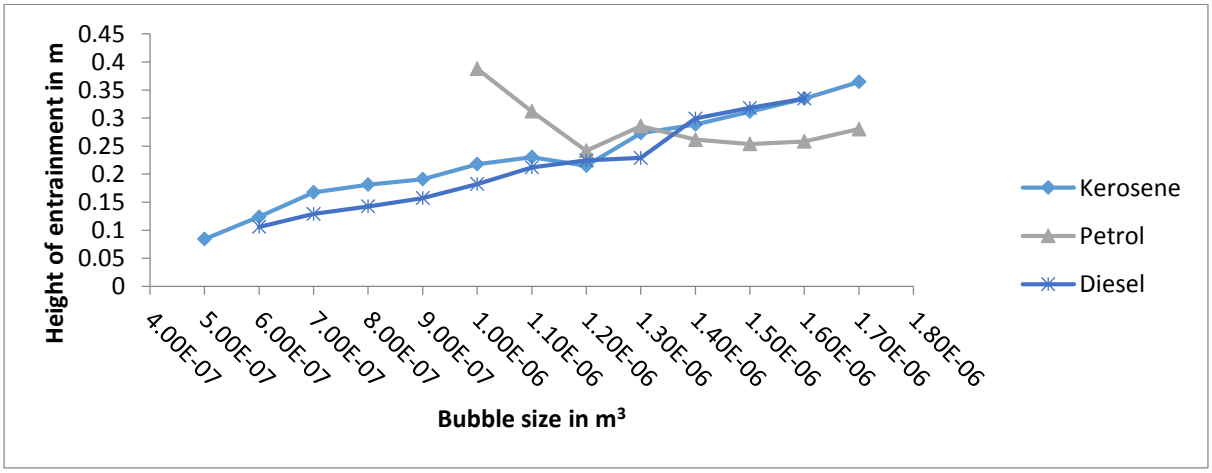

Graph 4.9: Graph showing the effect of fluid pair for conduit dimension 70 mm × 70 mm

The trend shows differences for all three fluid pairs. The trend for petrol-water combination is decreasing first and slightly increasing. The trends for diesel-water combination and kerosene-water combination follow each other closely. The unique

behavior of petrol-water combination may be attributed to the lower density of petrol as compared to diesel and kerosene. Also, the surface tension of petrol is very small while that of diesel and kerosene are high.

4.4 Recognition of various stages of entrainment

The different stages of entrainment could be observed during the experimental runs. To represent these in a pictorial format, the pictures are provided below. Each picture contains frames stitched together showing the rise of bubble through the interface. **Figure *4.1*** is for kerosene-water, **Figure *4.2*** is for diesel-water and **Figure *4.3*** is for petrol-water. The frame rate is 30 fps, i.e. the time gap between each consecutive frame is 1/30th of a second.

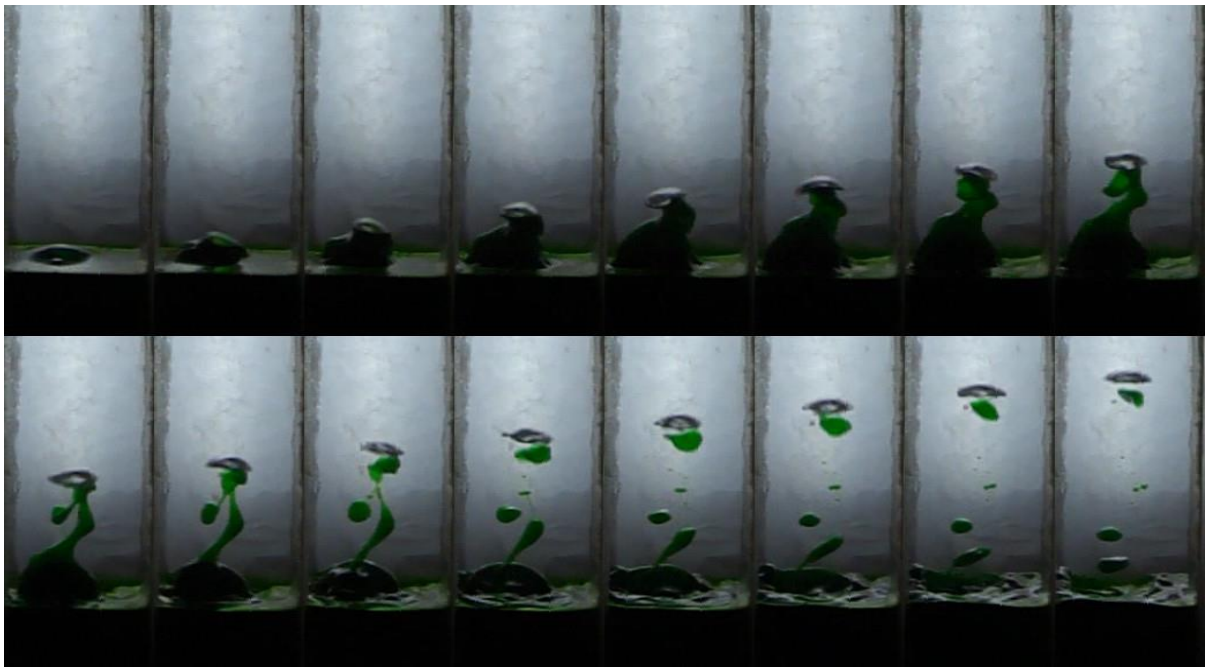

Figure 4.1: Frame-by-frame sequence with gap of 1/30th of a second showing stages of entrainment for conduit dimension 70 mm × 70 mm and fluid pair kerosene-water

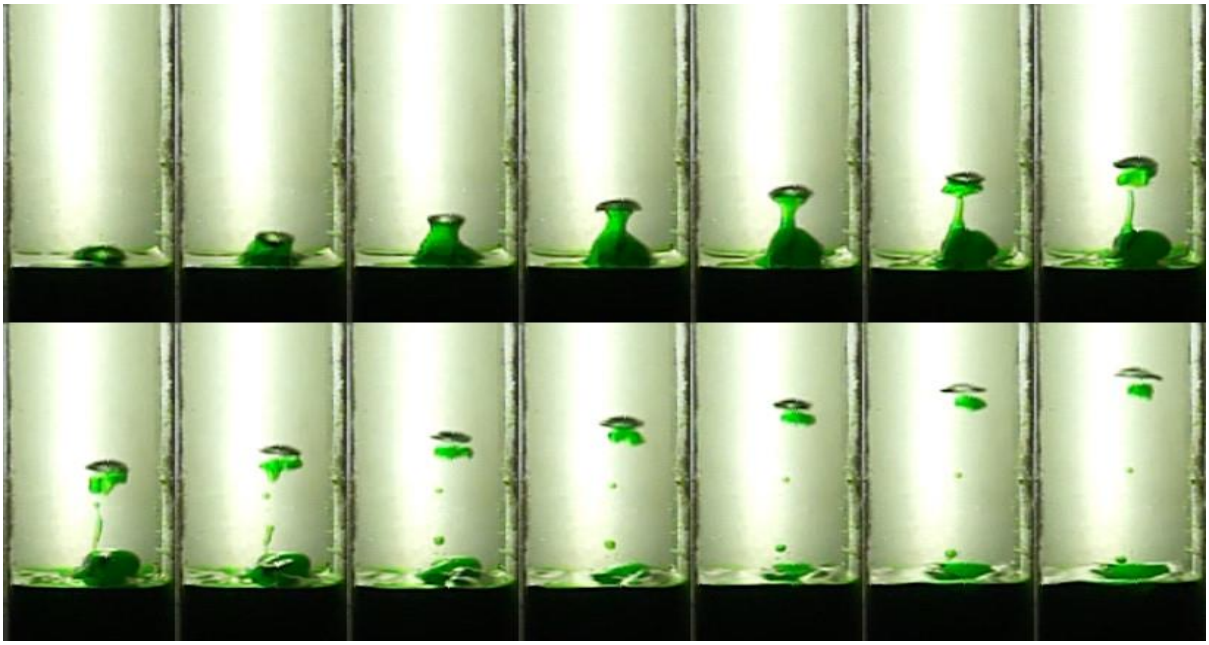

Figure 4.2: Frame-by-frame sequence with gap of 1/30th of a second showing stages of entrainment for conduit dimension 70 mm × 70 mm and fluid pair diesel-water

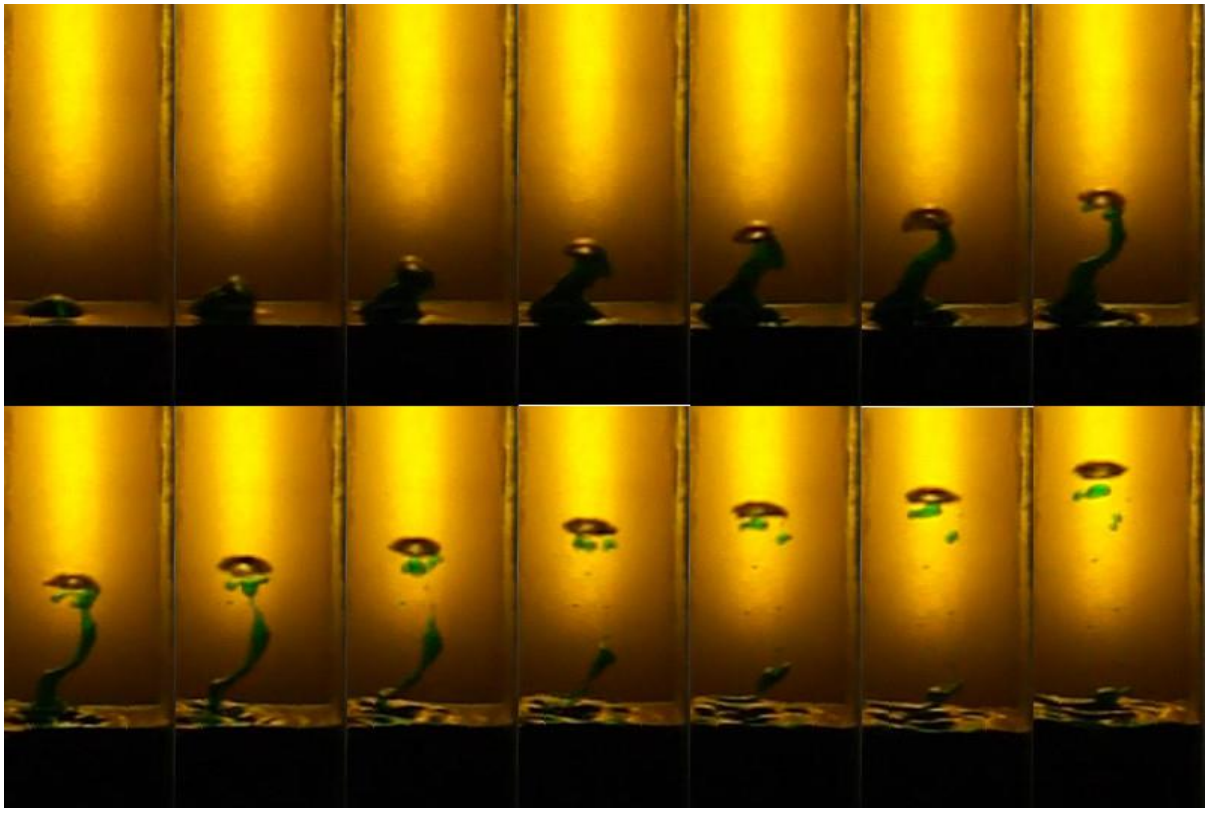

Figure 4.3: Frame-by-frame sequence with gap of 1/30th of a second showing stages of entrainment for conduit dimension 70 mm × 70 mm and fluid pair petrol-water

The stages can be identified easily. The identified stages are rise of stem [**Figure *4.4*** (**a**)], necking [**Figure *4.4*** (**b**)], snapping off of stem [**Figure *4.4*** (**c**)] and rise of separated drop [**Figure *4.4*** (**d**)].

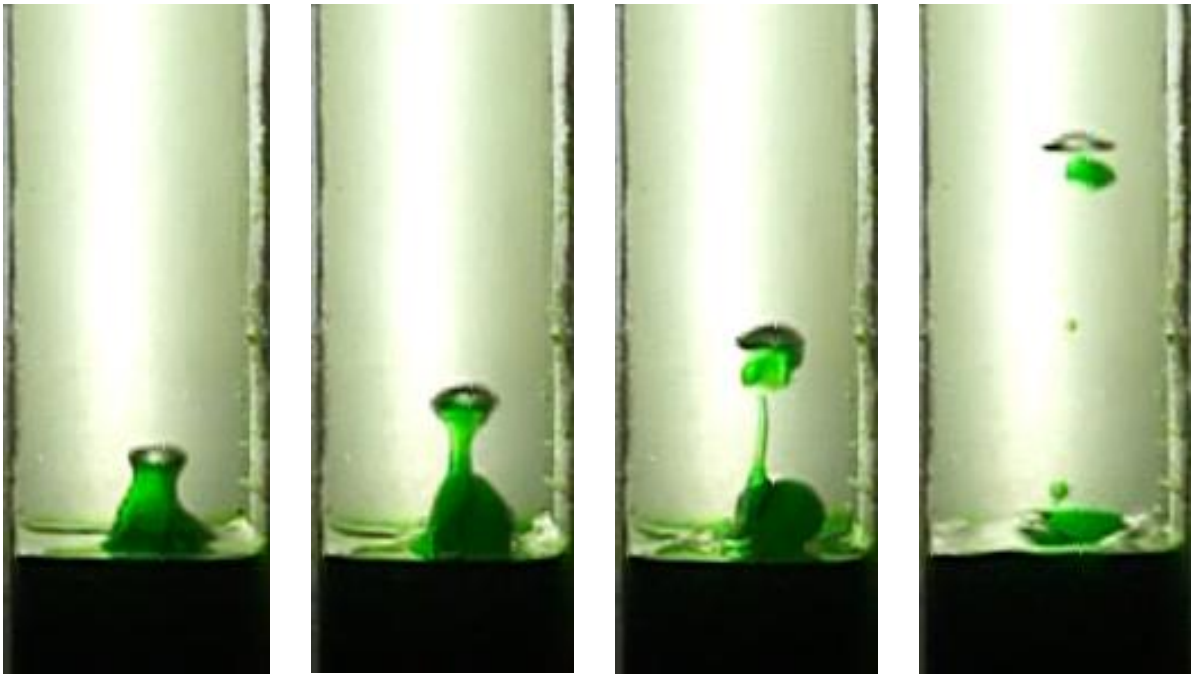

(a) **(b)** **(c)** **(d)**

Figure 4.4: Different stages of entrainment (a) rise of stem, (b) necking, (c) snapping off of stem and (d) rise of separated drop.

4.5 Simulation results

The phenomenon has been numerically simulated in 2D using commercial software Ansys. The mesh and geometry were created in mesher and design modeller inbuilt in ANSYS, while the problem was solved by using ANSYS workbench. The different stages of entrainment observed by the simulation are shown in **Figure *4.5***. The gap between each consecutive frame is 0.033 second, which is roughly equal to $1/30^{th}$ of a second, the frame rate at which the phenomenon was physically recorded from the

experiment. The stages observed from the simulation are the same as that observed from experimental runs.

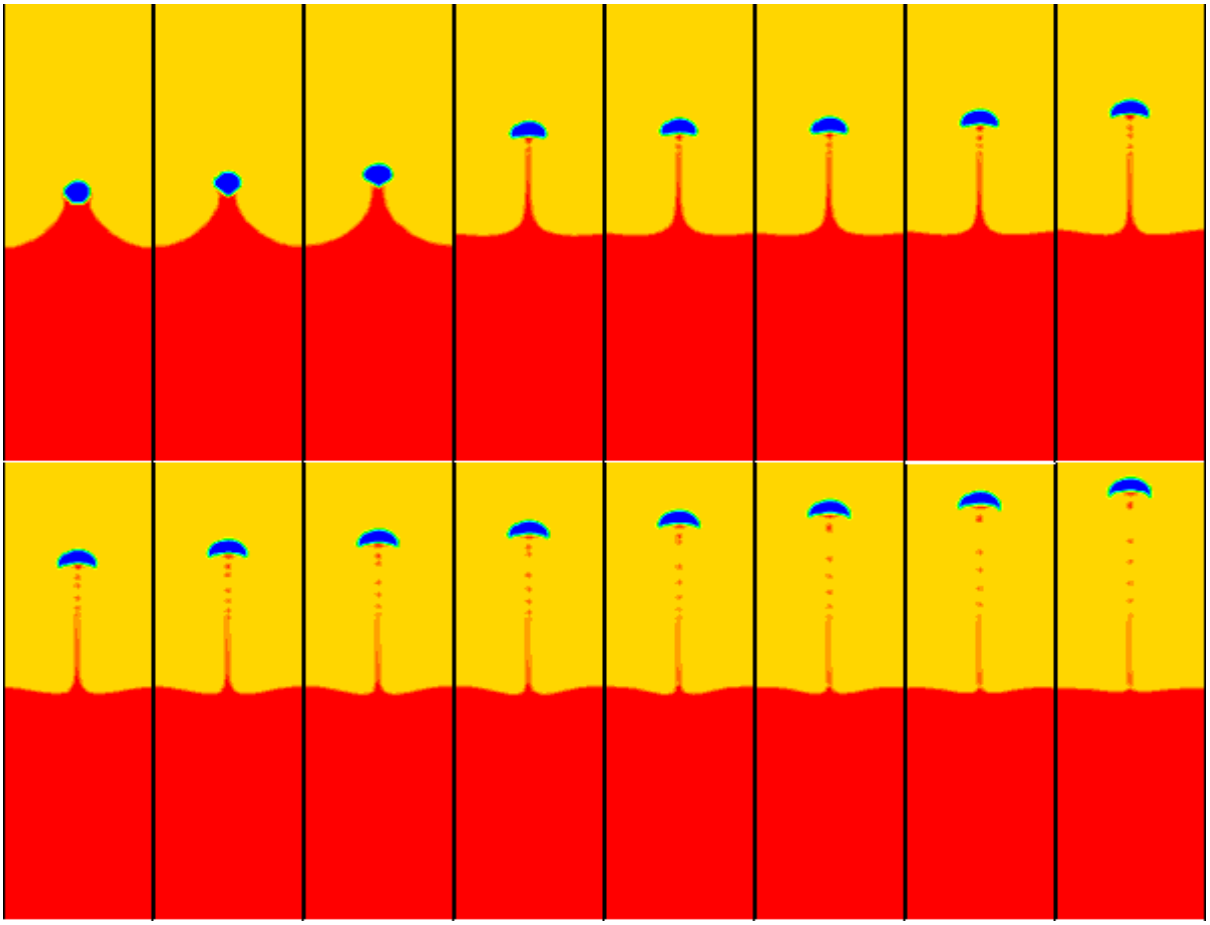

Figure 4.5: Frame-by-frame density contours with gap of 0.033 second obtained from simulation showing stages of entrainment for conduit dimension 70 mm × 70 mm and fluid pair kerosene-water

4.6 Comparison of results obtained experimentally and from simulation

The results from the simulation and experiment can be compared in the following **Figure *4.6***. This figure show the different stages identified in entrainment. The comparison is done by showing each of the stages obtained both experimentally via video recording and numerically by simulation in ANSYS. The comparison shows that the simulation and experimental observations tally with each other. Also, the sequence of stages followed is the same in both.

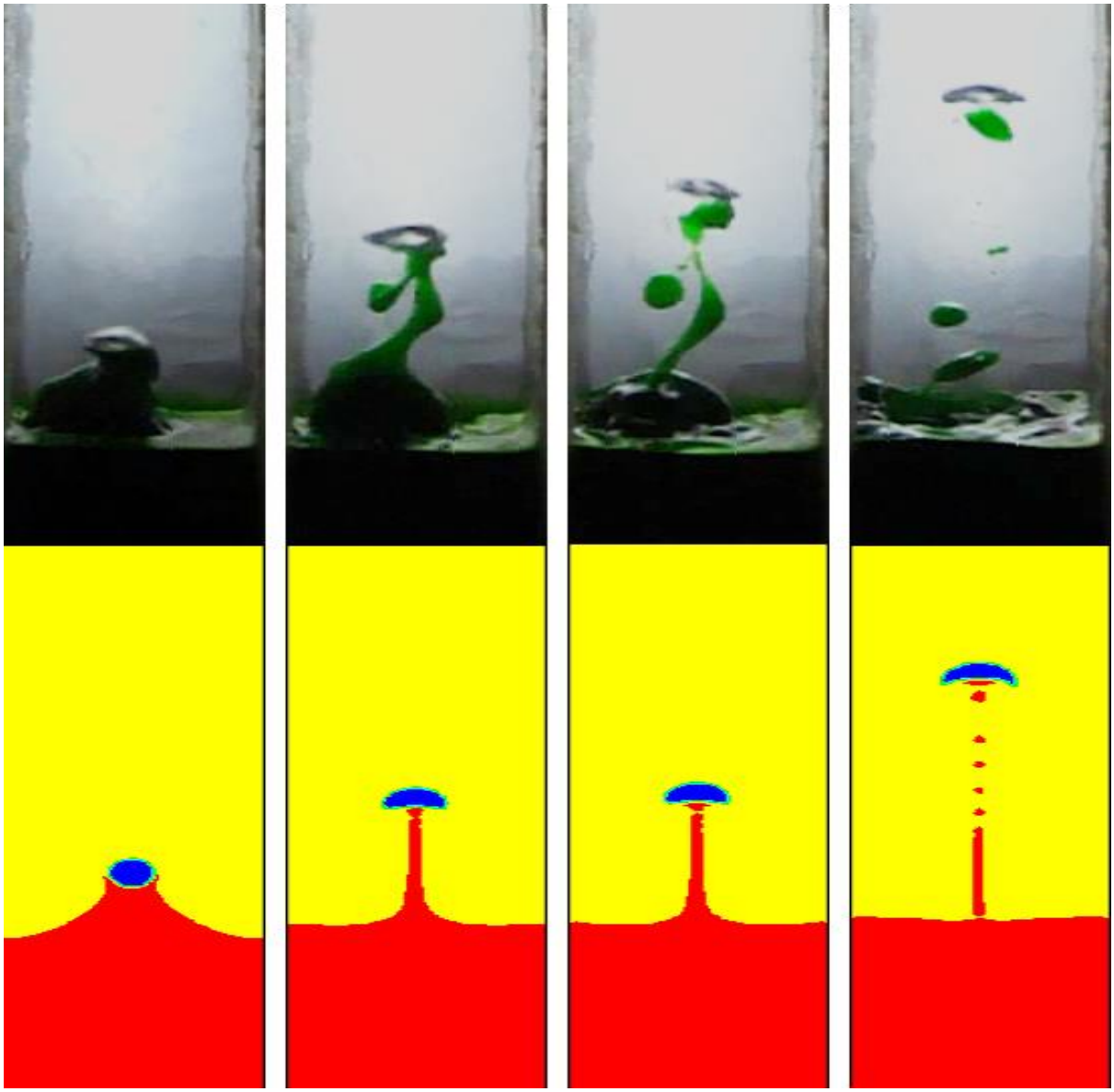

Figure 4.6: Comparison of different stages of entrainment as observed in experiment with the stages observed via simulation

4.7 Possible sources of Error

In each experiment, there are always some sources of error present. These may be insignificant, or they may have adverse effect on the results. However, it is advisable to be aware of all possible sources of error that may creep in. Some of the sources of error that may have occurred in this experiment are explained below.

Environment conditions vary. The temperature varies from duration to duration, thus it may affect the fluid properties. This change can lead to variations in the results. The bubble volume accuracy is limited by the syringe accuracy. The least count of the syringe is 0.1ml and hence all bubble volume measurements are accurate to 0.1ml. The bubble release mechanism is turned by hand to release the bubble. The speed of turning varied slightly from run to run as it is not humanly possible to maintain the exact speed repeatedly. This error was avoided by taking 5 experimental runs for each combination and then taking the average. This also eliminates random error. The height measurement is done by converting the pixel value to physical value. Thus, the accuracy of the height depends on the resolution of the camera. Since the video resolution used is sufficiently high (1280p × 720p), the occurrence of this error should be negligible. Dust can be observed to settle in the interface if the setup is left undisturbed for durations longer than 24 hours. This dust layer can lead to error and may prevent the bubble from crossing the interface. This dust may be undissolved particles in dye. To avoid this, the setup was cleaned and reset before continuation of experiment after a long break.

5 CONCLUSION

This section concludes the results obtained in this work. All the major observations and the conclusion drawn from them are presented here in a condensed form.

5.1 Increase in entrainment height with increase in bubble volume.

The different trends have been observed by plotting of graphs. The general trend noted is that the entrainment height increases with increase in bubble volume. The only exception is petrol-water fluid pair, where the height of entrainment decreases rapidly, reaches a minimum and then slowly increases with increase in bubble volume.

5.2 Range of bubble volumes.

The range of bubble volumes available for each combination of fluid pair and conduit dimension varies. The lower limit of this range is decided by the minimum bubble volume that can cause entrainment. The upper limit of this range is experimental setup limitation. The experimental setup cannot be created with much height as the setup tends to become unstable soon. The case of kerosene-water and diesel-water are almost similar. The variation in properties between kerosene and diesel is less. Hence, the bubble range for both are almost same. The properties of petrol are in stark contrast to kerosene and diesel, most remarkably in terms of surface tension and density. Thus, the bubble range for petrol-water pair is less than that of kerosene-water and diesel-water pairs. This can be attributed to the extremely low surface tension and comparatively low density of petrol.

5.3 Comparison of stages for 3 fluid pairs

The comparison for the different stages for three fluid pairs in a single conduit dimension has been shown in **Figure *4.1***, **Figure *4.2*** and **Figure *4.3*** in results section. Each frame is in time gap of $1/30^{th}$ of a second. The stem in kerosene-water pair is thick initially and then thins out later. The stem in diesel-water is thicker initially, but is short and then thins out quickly. The stem in petrol is thinner and gets longer and thinner before breaking off.

5.4 Petrol bubble oscillation

One of the observations unique to petrol is the trajectory of the bubble. The bubble rises rapidly and oscillates slightly while rising upwards. This again can be attributed to the lower density and extremely low surface tension of petrol when compared with kerosene

and diesel. Hence, such bubble oscillations are not noticed in cases of kerosene and diesel.

5.5 Diesel entrained water falls slowly

The entrained volume is observed to fall slowly and with stability in diesel. This may be due to the viscosity of diesel. This is not observed in either kerosene or petrol.

5.6 Simulation results

The different sequence of stages are shown in time gaps of 0.033 seconds in **Figure *4.5*** in results section. Since the assumption of 2D is taken during the simulations, the stages follow the real life observation but without the randomness. This comparison is shown in **Figure *4.6***.

REFERENCE

A.K. Roy, B. Maiti, PK. Das, Visualization of air entrainment by plunging jet, Procedia Engineering, volume 56, 2013, pp 468-473;

A.L. Kulkarni, a.W Patwardhan, CFD Modeling of gas entrainment in stirred tank systems, Chemical Engineering Research and Design, October 2013;

Denis Brouilliot, Pierre Lubin, Numerical simulations of air entrainment in a plunging jet of liquid, Journal of Fluids and Structures, Volume 43, November 2013, pp 428-440;

Di Liu, Yongjun Peng, Reducing the entrainment of clay minerals in flotation using tap and saline water, Powder Technology, Volume 253, February 2014, pp 216-222;

G.A. Greene, J.C. Chen & M.T. Conlin, Bubble induced entrainment between stratified liquid layers, International Journal of Heat and Mass Transfer, Volume 34, 1991, pp 149-157;

G.A. Greene, J.C. Chen & M.T. Conlin, Onset of entrainment between immiscible liquid layers due to rising gas bubbles, International Journal of Heat and Mass Transfer, Vol. 31, 1988, pp 1309-1317;

H. Shahrokhi & J.M. Shaw, The origin of fine drops in batch gas-agitated liquid-liquid systems, Chemical Engineering Science, Volume 49, 1994, pp 5203-5213;

Hongqiang Li, Qiming Feng, Siyuan Yang, Leming Ou, Ying Lu, The entrainment behavior of sericite in microcrystalline graphite flotation, Int. J. of Mineral Processing, Volume 127, March 2014, pp 1-9;

Ke Wang, Bofeng Bai, Weimin Ma, A model for droplet entrainment in churn flow, Chemical Engineering Science, Volume 104, December 2013, pp 1045-1055;

Ke Wang, Bofeng Bai, Weimin Ma, Huge wave and drop entrainment mechanism in gas-liquid churn flow, Chemical Engineering Science, Volume 104, December 2013, pp 638-646;

Luca Cristofano, Matteo Nobili, Gianfranco Caruso, Experimental study on unstable free surface vortices and gas entrainment onset conditions, Experimental Thermal and Fluid

Science, volume 52, January 2014, pp 221-229;

Shin Mei Tan, Hoon Kiat Ng, Suyin Gan, CFD modelling of soot entrainment via thermophoretic deposition and crevice flow in a diesel engine, Journal of Aerosol Science, Volume 66, December 2013, pp 83-95;

Xiu-Sahn Tian, Hui zhao, Hai-Feng Liu, Wei-Feng Li, Jian-Liang Xu, Liquid entrainment behavior at the nozzle exit in coaxial gas-liquid jets, Chemical Engineering Science, Volume 107, April 2014, pp 93-101;

Yasushi Oka, Jun-ichi Yamaguchi, Ko Muraoka, Decrease of carbon dioxide concentration and entrainment of horizontally spreading ceiling jet, Fire Safety Journal, Volume 63, January 2014, pp 37-42;

Zhaoming Meng, Laishun Wang, Wenxi Tian, Suizheng Qiu, Guanghui Su, Entrainment at T-junction: A review work, Progress in Nuclear Energy, volume 70, January 2014, pp 221-241;